J Infrared Milli Terahz Waves (2025) 46:1
https://doi.org/10.1007/s10762-024-01022-8

RESEARCH

High Azimuthal Mode Selectivity of a Cavity with Mode-Joining Corrugations for High-Harmonic Gyrotrons

Vitalii I. Shcherbinin[1,2] · **Tetiana I. Tkachova**[2] · **Anton V. Hlushchenko**[2] · **Yoshinori Tatematsu**[3] · **Manfred Thumm**[1] · **John Jelonnek**[1]

Received: 5 April 2024 / Accepted: 29 October 2024

Abstract

Mode-joining longitudinal corrugations are studied as a means of high azimuthal mode selectivity for cavities of high-harmonic terahertz gyrotrons. Their number dictates the choice of the jointed operating mode, which has a form of strongly coupled co- and counter-rotating azimuthal harmonics. It is found that the distinctive feature of this mode is a weak dependence of eigenvalue and ohmic losses on corrugation size. First, this favors the use of mode-joining corrugations with variable depth for efficient suppression of all competing modes by both diffractive and ohmic losses in the gyrotron cavity. Second, this provides a good robustness of gyrotron performance against manufacturing errors in the size of corrugations and only a minor conversion of the operating mode to spurious modes at junctions of the corrugated cavity with smooth-walled waveguides. The beneficial properties of mode-joining corrugations are demonstrated by a cavity design for a gyrotron operated in the second-harmonic $TE_{\pm 9,4}$ and third-harmonic $TE_{\pm 18,4}$ modes at 398 GHz and 593 GHz, respectively.

Keywords Gyrotron · Cyclotron harmonic · Cavity · Corrugations · Mode selectivity

✉ Vitalii I. Shcherbinin
vshch@ukr.net

[1] Institute for Pulsed Power and Microwave Technology, Karlsruhe Institute of Technology, 76131 Karlsruhe, Germany

[2] National Science Center "Kharkiv Institute of Physics and Technology", Kharkiv 61108, Ukraine

[3] Research Center for Development of Far-Infrared Region, University of Fukui, Fukui 910-8507, Japan

Published online: 20 November 2024

1 Introduction

Continuous-wave high-harmonic gyrotrons with relatively compact and reasonably priced superconducting magnets are highly demanded by many applications in the terahertz frequency range. However, increase in the harmonic number of the operating mode makes the problem of mode competition in a gyrotron cavity increasingly challenging [1].

One possible way to solve this problem is to equip the gyrotron cavity with selective structural elements, like wall steps [2, 3], grooves [4], irises [5, 6], impedance [7, 8] or mode-converting corrugations [9–11], coaxial insert [11–15], etc. Ideally, the selective element is required to efficiently suppress all competing modes in the cavity, be manufacturable, add no much complexity to the gyrotron design, provide good robustness of gyrotron performance against manufacturing errors and induce only a slight degradation in output mode purity, ohmic losses, and beam-wave interaction strength of the operating mode. Actually, it is not an easy matter to find a selective element, which is capable of meeting all these requirements simultaneously.

In this study, we introduce mode-joining corrugations and investigate their capacity to meet requirements imposed on selective elements for gyrotron cavities. As a generalized example, we consider the design of a corrugated cavity for a gyrotron with two operating modes, namely the second-harmonic mode at 398 GHz and the third-harmonic mode at 593 GHz. Such a dual-harmonic gyrotron is particularly attractive as a cost-efficient radiation source for terahertz applications.

2 Mode-Joining Corrugations

First, TE modes of a corrugated cylindrical metal waveguide of radius *R* are considered. The waveguide involves *N* periodic wedge-shaped longitudinal corrugations of width *w* and depth *d* (see the inset of Fig. 1).

Using the spatial harmonic method [9, 10, 16], a full-wave solution of the waveguide problem is found in the form of coupled azimuthal Bloch harmonics inside the guiding channel ($r < R$) and Fourier harmonics inside the corrugations. Coupled

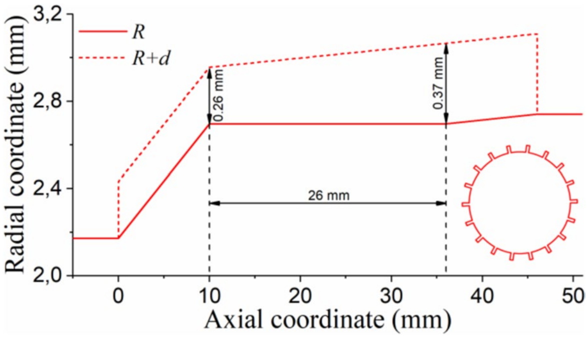

Fig. 1 Design of a cavity with profiled mode-joining corrugations

Bloch harmonics are characterized by azimuthal indices $m_j = m + jN$, where $j = 0, \pm 1, \pm 2\ldots$ is the harmonic number. When either or both w and d approach zero, Bloch harmonics transform to uncoupled $TE_{m_j,n}$ modes of a smooth-walled cylindrical waveguide.

In general, a coupling of Bloch harmonics has an intricate dependence on size and number of corrugations [9, 10]. Therefore, its strength is difficult to estimate in advance. However, one can expect a distinct coupling of Bloch harmonics of the corrugated waveguide, provided that the corresponding $TE_{m_j,n}$ modes of the smooth-walled waveguide have fairly close eigenvalues χ (cutoff frequencies $f_c = c\chi/(2\pi R)$).

It is well know that in smooth-walled cylindrical waveguides, degenerate modes with the same eigenvalue are co- ($m > 0$) and counter ($m < 0$) -rotating $TE_{m,\,n}$ modes. Clearly, a coupling of corresponding Bloch harmonics of the corrugated waveguide requires a natural number of corrugations N being equal to $2m/j$.

Of concern to us are waveguide modes with $m = \pm 9$ and $m = \pm 18$. For these modes, coupling of co- and counter-rotating Bloch harmonics can be achieved by choosing $N = 18$. For $N = 18$, $w = 0.15$ mm and $R = 2.696$ mm, the cutoff frequencies of modes with $m = \pm 18$ and $m = \pm 9$ as functions of corrugation depth d are shown in Fig. 2(a) and (b), where curves are labelled by the azimuthal m and radial n indices of $TE_{m,\,n}$ modes of the smooth-walled ($d = 0$) cylindrical waveguide. It can be seen that corrugations remove the degeneracy of co- and counter-rotating modes due to harmonic coupling. For each radial index n there are two modes with distinct cutoff frequencies (see also Fig. 5 in [17]). One mode behaves like the ordinary mode of a corrugated waveguide (see also Fig. 2(c) and (d)). Its cutoff frequency decreases with increasing d [9, 10]. The other mode has two distinct features. First, inside corrugations it has low field concentration caused by high-order Fourier harmonics (Fig. 3). For this reason, this mode is weakly sensitive to the corrugation depth. Second, inside the guiding channel, it involves an equally-weighted combination of co- and counter-rotating Bloch harmonics, each with nearly 50% of mode purity. Because of this, in the following, such a mode will be called a jointed mode designated as $TE_{\pm m,\,n}$ mode.

Formation of the jointed mode can be disturbed by interaction with other Bloch harmonics. For $m = \pm 9$ and $N = 18 = 2|m|$, such harmonics have $|m_j| \geq 3|m|$. Interaction with these harmonics is forbidden for $TE_{\pm m,\,n}$ modes subject to the condition $\chi < 3|m|$ [16], which is fulfilled for modes shown in Fig. 2(b). However, it should be noted that this condition is not mandatory and such harmonic interaction is absent for all jointed modes with enough large frequency separation from neighbouring $TE_{m_j,n}$ modes. In particular, this is true for the $TE_{\pm 18,\,4}$ mode and $N = 18 = |m|$, what can be seen in Fig. 2(a).

Figure 4 shows the influence of w and d on cutoff frequency and ohmic Q-factor of the $TE_{\pm 18,\,4}$mode of the corrugated copper waveguide with realistic electrical conductivity 2.9×10^7 S/m. It can be seen that, for small corrugation width w, the effect of corrugations on the jointed mode is minor. As w increases, the cutoff frequency and ohmic losses of the $TE_{\pm 18,\,4}$ mode increase. The effect of corrugation width on waveguide modes is more pronounced with increasing ratio between the width w and cutoff wavelength $\lambda_c = c/f_c$.

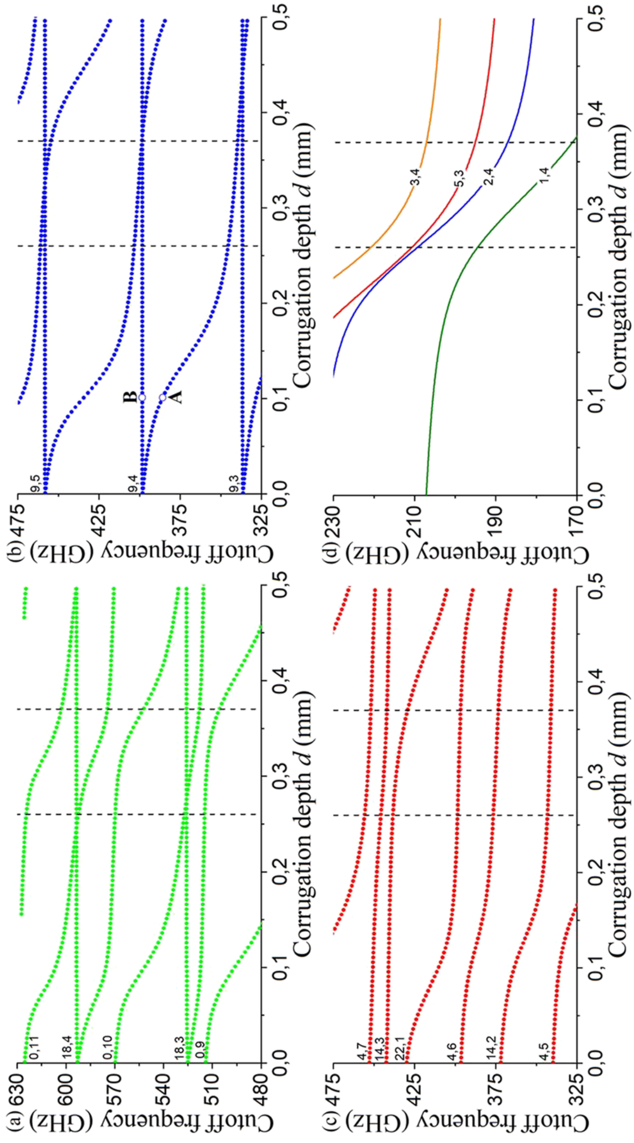

Fig. 2 Cutoff frequencies of TE modes with **(a)** $m = \pm 18$, **(b)** $m = \pm 9$, **(c)** $m = 4$ and **(d)** $m = 1, 2, 3, 5$ of a corrugated waveguide versus the depth d for $N = 18$, $w = 0.15$ mm and $R = 2.696$ mm

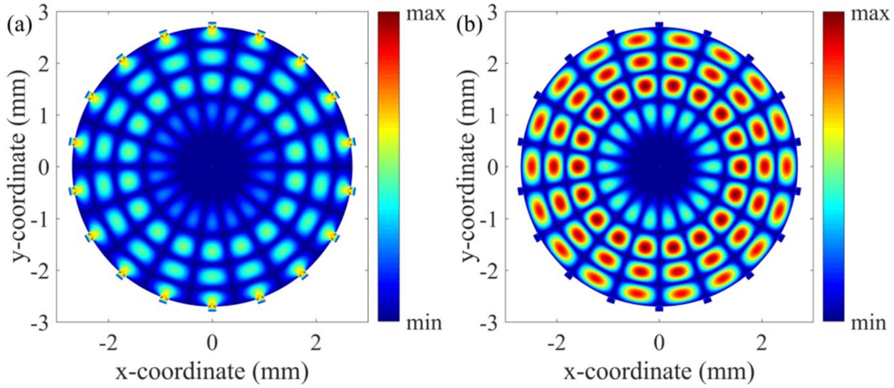

Fig. 3 Distribution of the azimuthal electric field over the transverse cross-section of the corrugated waveguide for modes shown by markers (**a**) A and (**b**) B in Fig. 2b

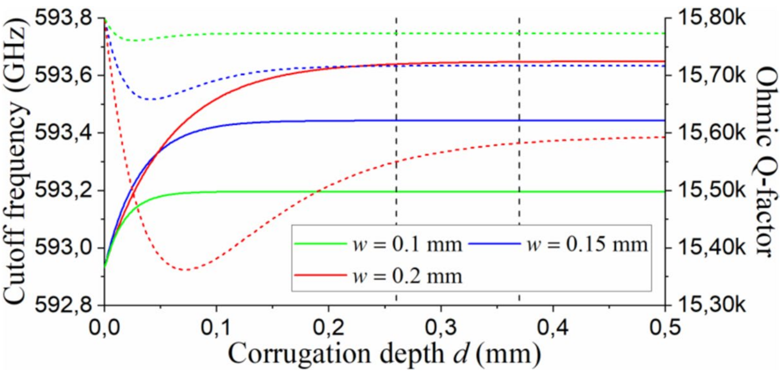

Fig. 4 Cutoff frequency (solid lines) and ohmic quality factor (dashed lines) of the $TE_{\pm 18,4}$ mode as functions of the corrugation depth *d* for different width *w*

Specific features of mode-joining corrugations make them particularly suitable for suppression of all waveguide modes, except for jointed modes with selected azimuthal indices *m*. First, such azimuthal mode selection is favoured by additional ohmic losses introduced by the corrugations. These losses for ordinary modes are much larger than those for jointed modes. Second, unlike jointed modes, ordinary modes of the corrugated waveguide possess cutoff frequencies (Fig. 2(c) and (d)), which depend on the corrugation depth. In a gyrotron cavity, this provides a means for suppression of all ordinary modes by diffractive losses induced by profiled mode-joining corrugations with variable depth.

Table 1 Cold characteristics of the smooth-walled cavity (d = 0)

Mode	$TE_{18,4}$	$TE_{9,4}$	$TE_{4,6}$	$TE_{5,2}$
f (GHz)	592.95	398.25	396.48	186.24
Q_{dif}	134300	49400	48950	7600
Q_{ohm}	15800	15300	17600	9650
Q_{tot}	14140	11680	12940	4270
L_{eff} (mm)	27.8	28.5	28.5	30.6

Table 2 Cold characteristics of the corrugated cavity

Mode	$TE_{\pm18,4}$	$TE_{\pm9,4}$	$TE_{4,6}$	$TE_{5,3}$
f (GHz)	593.48	398.44	397.19	196.26
Q_{dif}	134700	49900	1380	720
Q_{ohm}	15700	15300	14000	3370
Q_{tot}	14080	11700	1260	600
L_{eff} (mm)	27.9	28.6	17.5	13
η_p (%)	99.97	99.99	94.06	56.57

3 Cold-Cavity Calculations

To show this, we start with the cold (without an electron beam) gyrotron cavity with profiled mode-joining corrugations (Fig. 1). The cavity consists of a resonator with the radius $R = 2.696$ mm and length $L = 26$ mm, and input and output sections with taper angles 3° and 0.5°, respectively. The corrugations have the number $N = 18$, width $w = 0.15$ mm and continuously variable depth d. The corrugations depth is constant in the tapered input and output sections and increase linearly from 0.26 mm to 0.37 mm along the resonator length. The cavity has the electrical wall conductivity 2.9×10^7 S/m and is connected from both ends to uniform smooth-walled cylindrical waveguides. To take into account reflection and conversion of waveguide modes at the cavity ends, the coupled-mode approach of [8, 18, 19] is used.

Tables 1 and 2 list the characteristics of modes of the smooth-walled and corrugated cavities, respectively. It can be seen that, except for a frequency up-shift, corrugations produce only a slight effect on the jointed $TE_{\pm9,\,4}$ and $TE_{\pm18,\,4}$ modes, including their output mode purities η_p affected by mode coupling at the step transitions between the corrugated cavity and smooth-walled waveguides.

By contrast, corrugations provide strong discrimination against ordinary modes. First, ohmic losses of these modes greatly increase. This is particularly true for modes with cutoff wavelengths λ_c close to $4d$ [9, 10, 20]. Second, in the gyrotron cavity, profiled wall corrugations, similar to a tapered coaxial insert [11, 13, 15], give rise to additional diffractive losses of ordinary modes. This is because the cutoff frequencies of these modes decrease along the resonator length (Fig. 2). For this reason, their diffractive quality-factors Q_{dif} in the corrugated cavity are the same as those in a smooth-walled cavity with up-tapered resonator. Third, for the same reason, corrugations reduce the length of field localization inside the cavity (interaction cavity length L_{eff}) for ordinary modes. Thus, for these modes, corrugations are expected to initiate a large increase in starting currents, which are inversely proportional to $L_{eff}^2 Q_{tot}$ [1]. Note that, in just the same way, it is possible to suppress the jointed $TE_{\pm 9,\,4}$ mode, which transforms to an ordinary mode with the change in corrugation number N from 18 to 36.

Discrimination against ordinary modes can be adversely affected by mode coupling at the ends of the corrugated cavity. On the one hand, the mode coupling leads to a reduced output purity of ordinary modes. However, on the other hand, it can initiate strong mode reflection, which results in an increase of the diffractive quality factor. For example, such is the case with the ordinary $TE_{5,3}$ mode (Table 2).

Next we consider possible manufacturing errors in size of corrugations. We assume that corrugation depth and width are continuously variable and vary along the resonator length from $\delta_d + 0.26$ mm to 0.37 mm and $\delta_w + 0.15$ mm to 0.15 mm, respectively. The effect of δ_d and δ_w on frequency and total quality factor of the jointed $TE_{\pm 18,\,4}$ mode is shown in Fig. 5. As expected, this mode is mainly affected by the error δ_w. Assumed error δ_w leads to a non-uniform width of corrugations, which initiate variation in the cutoff frequency of the $TE_{\pm 18,\,4}$ mode along the resonator length (Fig. 4). For this reason, in addition to frequency and ohmic quality factor Q_{ohm}, the diffractive quality factor Q_{dif} of the jointed mode is affected by δ_w. For error $\delta_w = \pm 5$ µm, this leads to about 2 % change in the total quality factor Q_{tot} and power losses $(1 - Q_{tot}/Q_{dif})$ of the $TE_{\pm 18,\,4}$ mode.

4 Electron Beam-Wave Interaction Modeling

The $TE_{\pm 9,\,4}$ and $TE_{\pm 18,\,4}$ modes of the cavity with mode-joining corrugations are selected as second- and third-harmonic operating modes at 398 GHz and 593 GHz of a dual-harmonic gyrotron. The only reason is a minor competition between these modes. The gyrotron has the following parameters: electron beam current $I_b = 1$ A, beam voltage $V_b = 30$ kV, pitch factor $\alpha = 1.5$. The beam radius $r_b = 1.37$ mm is set close to the maximum strength of beam coupling with the co-rotating $TE_{18,\,4}$ mode. Velocity spread of beam electrons is assumed to be zero.

The dual-harmonic gyrotron is unfeasible without mode-joining corrugations. This can be seen in Fig. 6(a), which shows starting currents of selected operating modes and competing modes supported by the smooth-walled cylindrical cavity

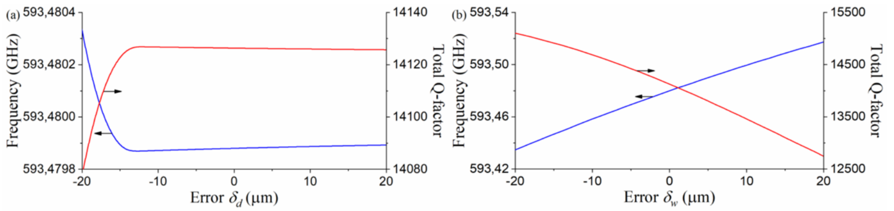

Fig. 5 The dependence of the cold-cavity frequency and total quality factor of the $TE_{\pm 18,4}$ mode on errors in (**a**) depth and (**b**) width of the mode-joining corrugations

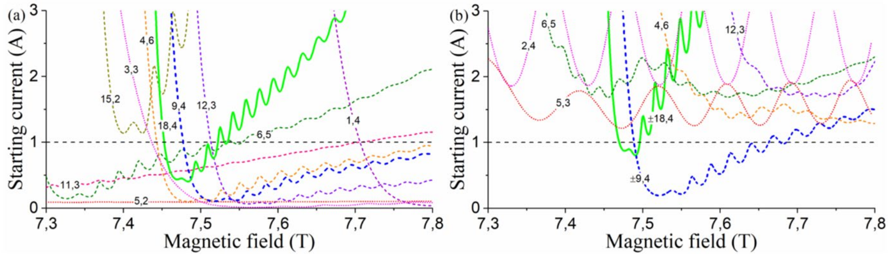

Fig. 6 Starting currents of the third- (solid line), second- (dashed lines) and first-harmonic (doted lined) modes supported by (**a**) the smooth-walled cavity and (**b**) cavity with profiled mode-joining corrugations

($d=0$). Clearly, competing modes present obstacles to operation of the dual-harmonic gyrotron. Among them is the first-harmonic $TE_{3,3}$ mode. The existence of this near-cutoff mode in the mode spectrum gives no way to avoid mode competition in the cavity by increasing velocity spread of beam electrons [21].

Mode-joining corrugations provide a means of suppressing all modes of the gyrotron cavity, except for the operating modes with desired azimuthal indices. Starting currents of these modes are shown in Fig. 6(b). It can be noticed that the starting currents of the operating $TE_{\pm9,\,4}$ and $TE_{\pm18,\,4}$ modes somewhat increase due to corrugations. This unfavourable effect is explained by reduced strength of beam interaction with mode-jointed modes, which are pairs of co- and counter-rotating Bloch harmonics with distinct beam-wave coupling coefficients [10]. Despite this fact, large increase in starting currents of competing modes makes the second-harmonic $TE_{\pm9,\,4}$ and third-harmonic $TE_{\pm18,\,4}$ modes the only modes, which can oscillate in the desired operating region.

Figure 7 shows the output power of the operating $TE_{\pm9,\,4}$ and $TE_{\pm18,\,4}$ modes versus the cavity magnetic field. It can be seen that oscillation regions of these modes are partially overlapped. This, however, is not critical for excitation of the operating modes. As a consequence, in the single-mode regime, the output power

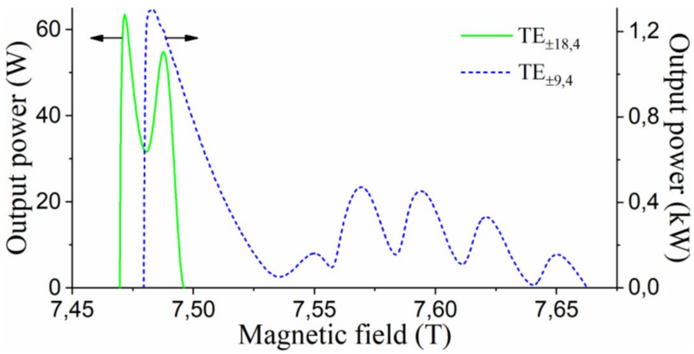

Fig. 7 Output power of the second- and third-harmonic operating modes at 398 GHz and 593 GHz, respectively

of the third-harmonic $TE_{\pm18,\,4}$ and second-harmonic $TE_{\pm9,\,4}$ modes exceed 60 W and 1 kW, respectively. For the $TE_{\pm9,\,4}$ mode with 1 kW output power, the peak ohmic loading in the corrugated cavity is about 1.2 kW/cm^2.

Finally, it is worth noting that the operating $TE_{\pm m,\,n}$ mode of the cavity with mode-joining corrugations is converted to uncoupled co- ($m > 0$) and counter ($m < 0$) -rotating $TE_{m,\,n}$ modes of the smooth-walled output waveguide. This property of the outgoing waves should be considered in the design of a high-performance quasi-optical output coupler for gyrotrons equipped with mode-joining corrugated cavities.

5 Conclusions

It has been shown that mode-joining corrugations enable high azimuthal mode selectivity of a gyrotron cavity. In such a cavity, the number of corrugations dictates the choice of the jointed operating mode, which has the form of an equally-weighted combination of co- and counter-rotating azimuthal harmonics. It has been found that this mode has unique properties due to low field concentration inside the corrugations. First, the operating mode features low ohmic losses induced by mode-joining corrugations. Second, its cutoff frequency depends only slightly on the corrugation depth and moderately on corrugation width. It has been shown that this provides a good robustness of gyrotron performance against errors in the corrugation size and a minor mode conversion at junctions of the corrugated cavity with smooth-walled waveguides. In this cavity, suppression of competing modes is favored by ohmic losses inside the corrugations and greatly enhanced by increased diffractive losses and reduced interaction cavity length, which are caused by tapering of the corrugation depth. It has been found that the only unwanted effect of such corrugations is the reduced strength of electron beam coupling with the jointed operating mode. A specific design has been made of a cavity with profiled mode-joining corrugations for a gyrotron operated in the second- and third-harmonic modes at 398 GHz and 593 GHz, respectively. It has been shown that corrugations initiate a large increase in starting currents of all competing modes and thereby provide a means for single-mode gyrotron operation at the second and third cyclotron harmonics.

Acknowledgements The work of V.I. Shcherbinin was supported by the Philipp Schwartz Initiative of the Alexander von Humboldt Foundation and International Collaborative Research Program of the Research Center for Development of Far-Infrared Region, University of Fukui, Japan.

Author contribution All authors contributed to the study conception and design. Material preparation, data collection and analysis were performed by V.S. The first draft of the manuscript was written by V.S. and all authors commented on previous versions of the manuscript. All authors read and approved the final manuscript.

Funding Open Access funding enabled and organized by Projekt DEAL. Financial support was received from the Philipp Schwartz Initiative of the Alexander von Humboldt Foundation and International Collaborative Research Program of the Research Center for Development of Far-Infrared Region, University of Fukui, Japan.

Data Availability No datasets were generated or analysed during the current study.

Declarations

Competing interests The authors declare no competing interests.

References

1. B.G. Danly, R.J. Temkin, Phys. Fluids (1986) DOI: https://doi.org/10.1063/1.865446
2. I.V. Bandurkin, Y.K. Kalynov, A.V. Savilov, Phys. Plasmas (2013) DOI: https://doi.org/10.1063/1.4775083
3. M.M. Melnikova, A.G. Rozhnev, N.M. Ryskin, Y. Tatematsu, M. Fukunari, Y. Yamaguchi, T. Saito, IEEE Trans. Electron Devices (2017) DOI: https://doi.org/10.1109/TED.2017.2764874
4. V. Bandurkin, M.Y. Glyavin, A.E. Fedotov, A.P. Fokin, M. Fukunari, I.V. Osharin, A.V. Savilov, D.Y. Shchegolkov, Y. Tatematsu, IEEE Trans. Electron Devices (2022) DOI: https://doi.org/10.1109/TED.2022.3142657
5. S. Spira-Hakkarainen, K.E. Kreischer, R.J. Temkin, IEEE Trans. Plasma Sci. (1990) DOI: https://doi.org/10.1109/27.55903
6. D. Sun, H. Chen, G. Ma, W. Lei, H. Chen, F. Meng, J. Infrared Millim. Terahertz Waves (2014) DOI: https://doi.org/10.1007/s10762-014-0064-1
7. V.I. Shcherbinin, V.I. Tkachenko, J. Infrared Millim. Terahertz Waves (2017) DOI: https://doi.org/10.1007/s10762-017-0386-x
8. V.I. Shcherbinin, T.I. Tkachova, A.V. Maksimenko, M. Thumm, J. Jelonnek, J. Infrared Millim. Terahertz Waves (2022), DOI: https://doi.org/10.1007/s10762-022-00888-w
9. T.I. Tkachova, V.I. Shcherbinin, V.I. Tkachenko, J. Infrared Millim. Terahertz Waves (2019) DOI: https://doi.org/10.1007/s10762-019-00623-y
10. T.I. Tkachova, V.I. Shcherbinin, V.I. Tkachenko, Z.C. Ioannidis, M. Thumm, J. Jelonnek, J. Infrared Millim. Terahertz Waves (2021) DOI: https://doi.org/10.1007/s10762-021-00772-z
11. D. V. Peponis, K.A. Avramidis , I.G. Chelis , Z.C. Ioannidis, S. Illy , J. Jelonnek, G.P. Latsas, I.G. Tigelis, IEEE Trans. Electron Devices (2023) DOI: https://doi.org/10.1109/TED.2023.3326431
12. V.I. Shcherbinin, V.I. Tkachenko, K.A. Avramidis, J. Jelonnek, IEEE Trans. Electron Devices (2019) DOI: https://doi.org/10.1109/TED.2019.2944647
13. V.I. Shcherbinin, Y.K. Moskvitina, K.A. Avramidis, J. Jelonnek, IEEE Trans. Electron Devices (2020) DOI: https://doi.org/10.1109/TED.2020.2996179
14. V.I. Shcherbinin, K.A. Avramidis, M. Thumm, J. Jelonnek, J. Infrared Millim. Terahertz Waves (2021) DOI: https://doi.org/10.1007/s10762-020-00760-9
15. V.I. Shcherbinin, IEEE Trans. Electron Devices (2021) DOI: https://doi.org/10.1109/TED.2021.3090348
16. Z.C. Ioannidis, K.A. Avramides, G.P. Latsas, I.G. Tigelis, IEEE Trans. Plasma Sci. (2011) DOI: https://doi.org/10.1109/TPS.2011.2118766
17. I. Osharin, A. Savilov, D. Shchegolkov, Proc. Int. Vac. Electron. Conf. (IVEC) (2021) DOI: https://doi.org/10.1109/IVEC51707.2021.9722469
18. V.I. Shcherbinin, T.I. Tkachova, M. Thumm, J. Jelonnek, Proc. IEEE 2nd Ukr. Microw. Week (UkrMW) (2022) DOI: https://doi.org/10.1109/UkrMW58013.2022.10037054
19. V.I. Shcherbinin, T.I. Tkachova, O.L. Andrieieva, M. Thumm, J. Jelonnek, Proc. Int. Conf. Infrared Millim. Terahertz Waves (IRMMW-THz) (2023) DOI: https://doi.org/10.1109/IRMMW-THz57677.2023.10299166

20. V.I. Shcherbinin, B.A. Kochetov, A.V. Hlushchenko, V.I. Tkachenko, IEEE Trans. Microw. Theory Techn. (2019) DOI: https://doi.org/10.1109/TMTT.2018.2882493
21. I. Bandurkin, A. Fedotov, M. Glyavin, T. Idehara, A. Malkin, V. Manuilov, A. Sergeev, A. Tsvetkov, V. Zaslavsky, I. Zotova, IEEE Trans. Electron Devices (2020) DOI: https://doi.org/10.1109/TED.2020.3012524